doi:10.1016/j.jmb.2010.11.013 J. Mol. Biol. (2011) 405, 773–786

Contents lists available at www.sciencedirect.com

Journal of Molecular Biology

journal homepage: http://ees.elsevier.com.jmb

Critical Scaffolding Regions of the Tumor Suppressor Axin1 Are Natively Unfolded

Maria Noutsou[1], Afonso M. S. Duarte[2], Zeinab Anvarian[1], Tatiana Didenko[2], David P. Minde[2], Ineke Kuper[1], Isabel de Ridder[1], Christina Oikonomou[1], Assaf Friedler[3], Rolf Boelens[4], Stefan G. D. Rüdiger[2]* and Madelon M. Maurice[1]*

[1]*Department of Cell Biology, University Medical Center Utrecht, Utrecht, The Netherlands*
[2]*Cellular Protein Chemistry, Bijvoet Center for Biomolecular Research, Utrecht University, Utrecht, The Netherlands*
[3]*Department of Organic Chemistry, The Hebrew University of Jerusalem, Jerusalem, Israel*
[4]*Biomolecular NMR Spectroscopy, Bijvoet Center for Biomolecular Research, Utrecht University, Utrecht, The Netherlands*

Received 30 June 2010;
received in revised form
5 November 2010;
accepted 5 November 2010
Available online
16 November 2010

Edited by P. Wright

Keywords:
Wnt pathway;
natively unfolded;
scaffold;
Axin;
β-catenin degradation

The Wnt pathway tumor-suppressor protein Axin coordinates the formation of a critical multiprotein destruction complex that serves to downregulate β-catenin protein levels, thereby preventing target gene activation. Given the lack of structural information on some of the major functional parts of Axin, it remains unresolved how the recruitment and positioning of Wnt pathway kinases, such as glycogen synthase kinase 3β, are coordinated to bring about β-catenin phosphorylation. Using various biochemical and biophysical methods, we demonstrate here that the central region of Axin that is implicated in binding glycogen synthase kinase 3β and β-catenin is natively unfolded. Our results support a model in which the unfolded nature of these critical scaffolding regions in Axin facilitates dynamic interactions with a kinase and its substrate, which in turn act upon each other.

Introduction

The Wnt/β-catenin signaling pathway controls essential cellular decisions on growth and differentiation during embryonic development and in adult tissue homeostasis.[1] Inappropriate activation of the Wnt pathway due to mutations is frequently linked to the development of cancer.[2] Molecular events in the Wnt pathway converge on the regulation of the protein levels of the transcriptional coactivator β-catenin, which controls key developmental gene expression programs.[3]

In the absence of Wnt ligand, the tumor-suppressor protein Axin coordinates the formation of a multiprotein complex composed of the scaffolding protein adenomatous polyposis coli (APC) and the kinases casein kinase 1 (CK1) and glycogen synthase kinase 3β (GSK3β).[4–8] This protein complex efficiently recruits and phosphorylates β-catenin on conserved N-terminal serine and threonine residues, thereby marking it for ubiquitin–proteasome-mediated

*Corresponding authors. E-mail addresses: s.g.d.rudiger@uu.nl; M.M.Maurice@umcutrecht.nl.

Abbreviations used: APC, adenomatous polyposis coli; CK1, casein kinase 1; GSK3β, glycogen synthase kinase 3β; AxinCR, central region of Axin; GST, glutathione *S*-transferase; siRNA, small interfering RNA; WCM, Wnt3a-conditioned medium; TFE, 2,2,2-trifluoroethanol; HSQC, heteronuclear single-quantum coherence; JNK, c-Jun N-terminal kinase; TEV, tobacco etch virus; TCEP, tris(2-carboxyethyl)phosphine; CV, column volumes; DSS, 2,2-dimethyl-2-silapentane-5-sulfonate.

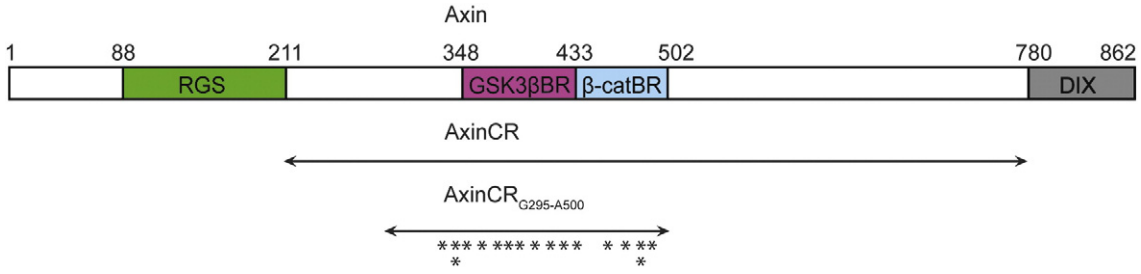

Fig. 1. Domain organization of Axin. Well-defined Axin domains that are important for Wnt pathway regulation are shown. The N-terminal RGS domain binds APC, and the C-terminal DIX domain is responsible for homodimerization and heterodimerization. The central region (indicated as AxinCR), connecting the RGS and DIX domains, binds to GSK3β and β-catenin. The experimental fragment AxinCR$_{G295-A500}$ is indicated. Asterisks indicate the locations of missense mutations in AxinCR reported in a variety of human tumors.[18–22]

degradation.[9–15] Wnt binding to its receptors Frizzled and Lrp5/6 at the cell surface results in the recruitment of the Axin–GSK3β complex, which now turns its activity to phosphorylate the cytoplasmic tail of Lrp6.[16,17] Together, these events lead to an accumulation of dephosphorylated β-catenin and its migration to the nucleus to induce target gene transcription.

Axin possesses multiple functional domains through which it orchestrates β-catenin phosphorylation (Fig. 1). The N-terminal RGS (*r*egulator of *G*-protein *s*ignaling) domain mediates binding to the large scaffolding protein APC. APC itself carries three short Axin binding motifs and multiple binding sites for β-catenin.[23] The C-terminal DIX domain of Axin mediates self-association and binding to the DIX domain of Dishevelled, which is believed to modulate its signaling activity.[24–26] The central part of Axin contains binding sites for GSK3β, β-catenin, and CK1.[5,27] Scaffolding of APC, GSK3β, and β-catenin by Axin dramatically enhances GSK3β-mediated phosphorylation of β-catenin.[28,29] At the same time, GSK3β-mediated phosphorylation of Axin enhances its stability.[30]

While crystal structures are available for both the RGS domain and the DIX domain of Axin,[26,31] experimental structural information on the central region of Axin (AxinCR) is limited to small helical Axin peptides that were cocrystallized with GSK3β and β-catenin.[32,33] Insight into the structural properties of this region is crucial to understanding how Axin coordinates protein–protein interactions in the β-catenin destruction complex to mediate its tumor-suppressor activity. The functional importance of the Axin central region is illustrated by an increasing number of reported missense mutations in this part of the protein in various tumors (Fig. 1).[18–22]

Using various biophysical and biochemical methods, we demonstrate here that the central domain of Axin is intrinsically disordered. Our findings support a model in which crucial scaffolding functions of Axin are exerted by a large highly flexible region.

Results

Recombinant AxinCR$_{G295-A500}$ is functional *in vitro* and *in vivo*

Functional understanding of AxinCR, which connects the folded N-terminal RGS domain and the C-terminal DIX domain (Fig. 1), is limited due to a lack of experimental structural information. To determine the structural properties of AxinCR in an experimental approach, we generated and purified a recombinant fragment of AxinCR spanning Gly295 to Ala500 and including the GSK3β-binding domain and the β-catenin binding domain. First, we set out to determine if AxinCR$_{G295-A500}$, lacking the N-terminal RGS domain and the C-terminal DIX domain of Axin, is functional in isolation. We recombinantly produced GSK3β as His-tagged NusA fusion protein (to increase solubility) and His-tagged β-catenin. Both His-NusA-tagged GSK3β and His-tagged β-catenin, but not control His-NusA protein, were able to bind AxinCR$_{G295-A500}$ in a pull-down approach (Fig. 2a–c). To verify that this interaction also takes place *in vivo*, we expressed glutathione *S*-transferase (GST)-tagged AxinCR$_{G295-A500}$ in HEK293T cells and confirmed its binding to endogenous GSK3β and β-catenin (Fig. 2d). These results are consistent with current models, which propose that AxinCR is able to perform its scaffolding function by bringing together kinase and substrate. In addition, ectopic expression of the GST-tagged AxinCR$_{G295-A500}$ fragment in mammalian cells strongly induced β-catenin-mediated transcription in a luciferase reporter assay (TOPflash),[34] whereas the GST-tagged full-length Axin protein fully suppresses Wnt-induced activation (Fig. 2e). These findings suggest that the AxinCR$_{G295-A500}$ fragment competes with endogenous Axin (estimated ratio, 50:1) for binding to GSK3β and β-catenin, and dominantly

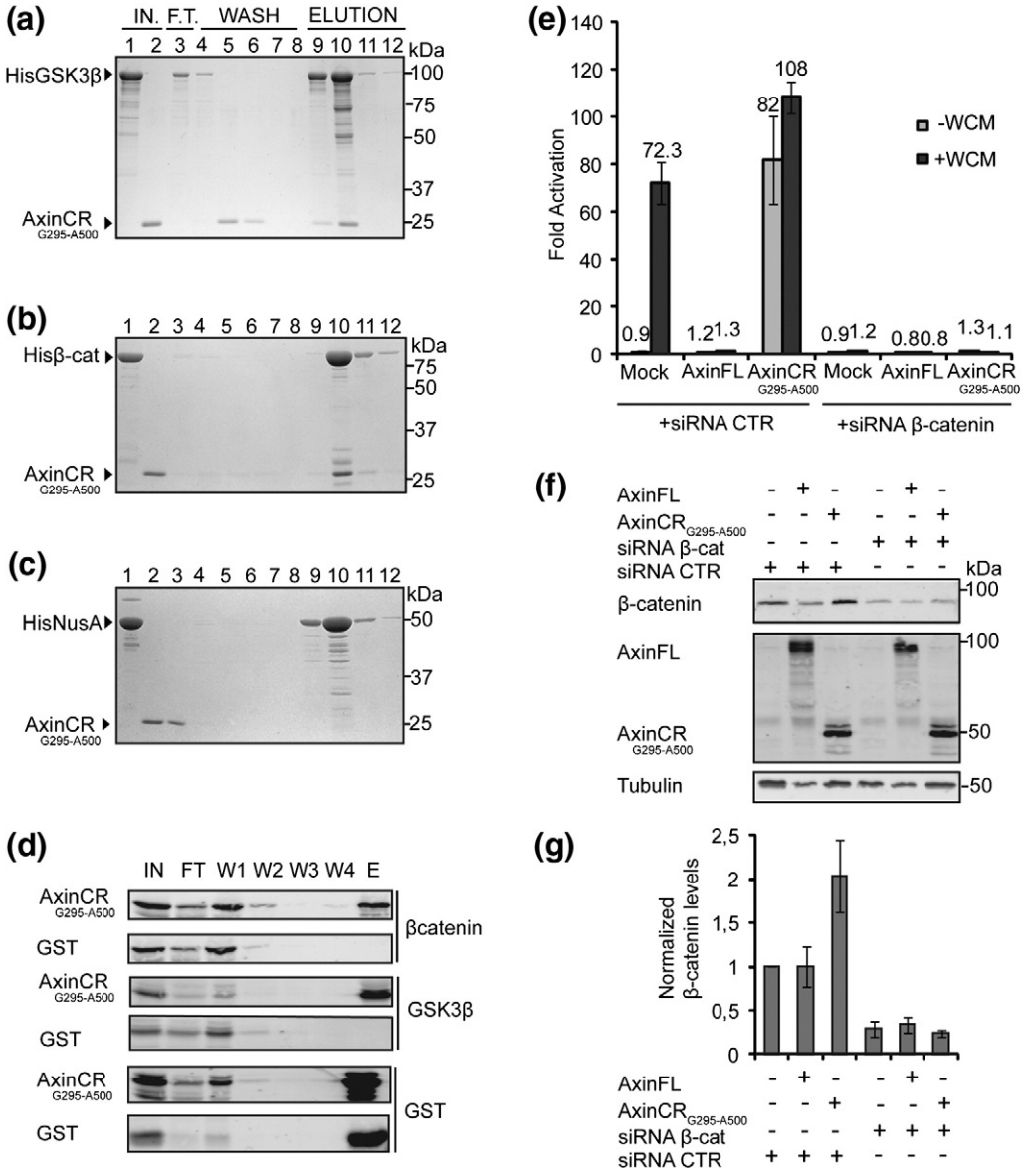

Fig. 2. AxinCR$_{G295\text{-}A500}$ binds GSK3β and β-catenin, and hyperactivates the Wnt pathway through activation of β-catenin. (a–c) AxinCR$_{G295\text{-}A500}$ forms a complex with GSK3β and β-catenin. His-NusA-GSK3β, His-β-catenin N138-L781, or His-NusA (lane 1; input) was incubated with purified AxinCR$_{G295\text{-}A500}$ (lane 2; input). Protein complexes were isolated with Ni-NTA beads in a pull-down assay. Flow-through (FT; lane 3), wash (lanes 4–8), and eluted (lanes 9–12) fractions are shown. AxinCR$_{G295\text{-}A500}$ coelutes with His-NusA-GSK3β (a) and His-β-catenin (b), but not with the tag protein His-NusA (c). (d) Lysates from HEK293T overexpressing GST or GST-AxinCR$_{G295\text{-}A500}$ were incubated with GST beads. Endogenous β-catenin and GSK3β coelute with GST-AxinCR$_{G295\text{-}A500}$, but not with GST alone. (e) TOPflash luciferase reporter activity induced in HEK293T cells expressing the control vector, GST-tagged full-length Axin (AxinFL), or GST-AxinCR$_{G295\text{-}A500}$. Cells were treated with β-catenin or control siRNA, and with WCM (+WCM) or control medium (−WCM), as indicated. Relative TOPflash/FOPflash luciferase ratios (±SD) of duplicate experiments are shown. Results represent at least three independent experiments. (f) Expression levels of β-catenin, AxinFL, AxinCR$_{G295\text{-}A500}$, and tubulin in the presence or in the absence of siRNA against β-catenin. (g) Quantification of β-catenin expression levels normalized against tubulin.

interferes with the formation of a functional endogenous destruction complex. As a consequence, β-catenin accumulates and translocates to the nucleus to initiate the transcription of the luciferase reporter gene. In concordance, TOPflash reporter activity is induced by AxinCR$_{G295\text{-}A500}$ in a Wnt-independent manner (Fig. 2e).

To verify that the TOPflash activity enhanced by AxinCR$_{G295\text{-}A500}$ expression in cells depends on the activation of β-catenin, we performed the TOPflash

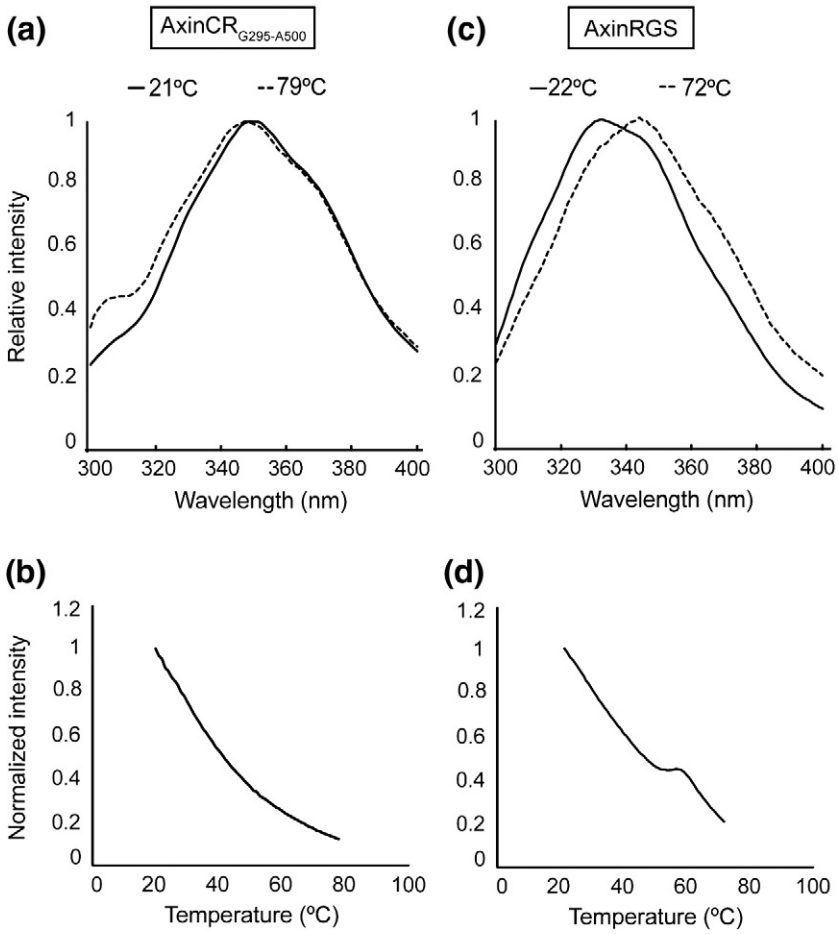

Fig. 3. AxinCR$_{G295-A500}$ does not undergo temperature-induced unfolding. (a) Fluorescence spectra of AxinCR$_{G295-A500}$ measured at low (21 °C) and high (79 °C) temperatures. Maximal spectral intensities were equalized for both temperatures to allow for a comparison of peak shifts. (b) Fluorescence intensity of AxinCR$_{G295-A500}$ during a stepwise temperature increase ranging from 21 °C to 79 °C at 352 nm. Fluorescence intensity values were normalized against values obtained at 20 °C. (c) Fluorescence spectra of AxinRGS measured at low (22 °C) and high (72 °C) temperatures. (d) Fluorescence intensity of AxinRGS during a stepwise temperature increase ranging from 22 °C to 72 °C at 340 nm. The mean values of three measurements are shown.

assay in the presence of small interfering RNA (siRNA) oligonucleotides that silence β-catenin expression (Fig. 2e). siRNA treatment for 48 h reduces endogenous β-catenin expression levels to 30% (Fig. 2f and g) and abrogates TOPflash activity in the presence or in the absence of AxinCR$_{G295-A500}$, as well as upon addition of Wnt3a-conditioned medium (WCM). These results argue that AxinCR$_{G295-A500}$ retains its GSK3β and β-catenin binding functions independent of the rest of the protein *in vivo* and *in vitro*.

AxinCR$_{G295-A500}$ does not undergo thermal denaturation and displays an extended conformation

To determine whether AxinCR$_{G295-A500}$ carries a three-dimensionally folded hydrophobic core, we performed thermal denaturation studies by monitoring intrinsic protein (Trp-mediated) fluorescence as a measure of tertiary structural changes. Two Trp residues are present in AxinCR$_{G295-A500}$ (W297 and W444). We monitored the fluorescence spectrum of AxinCR$_{G295-A500}$ while raising the temperature from 20 °C to 80 °C (Fig. 3a and b). The fluorescence intensity of AxinCR$_{G295-A500}$ peaked at similar wavelengths at minimal and maximal temperatures (Fig. 3a). In concordance, the thermal denaturation curve of AxinCR$_{G295-A500}$ did not reveal a transition in fluorescence intensity (Fig. 3b). In contrast, a recombinantly produced Axin RGS domain, which is known to exist in a tightly folded conformation,[31] significantly shifts in peak fluorescence intensity when comparing minimal and maximal temperatures (Fig. 3c). Moreover, the RGS domain yielded a clear transition in fluorescence intensity during thermal denaturation, reflecting an unfolding of the hydrophobic core (Fig. 3d). These findings indicate that AxinCR$_{G295-A500}$, in contrast to the Axin RGS domain, lacks folded domains with a hydrophobic core, or that the two Trp residues in the AxinCR$_{G295-A500}$ sequence are not inside any folded region. To assess whether AxinCR$_{G295-A500}$ lacks a hydrophobic core and consequently adopts an extended shape, we performed analytical size-exclusion chromatography (Fig. 4a). AxinCR$_{G295-A500}$ eluted from the column with an elution volume of 9.92 ml. According to the calibration curve of standard markers, this volume corresponds to a molecular mass of 70 kDa, a value

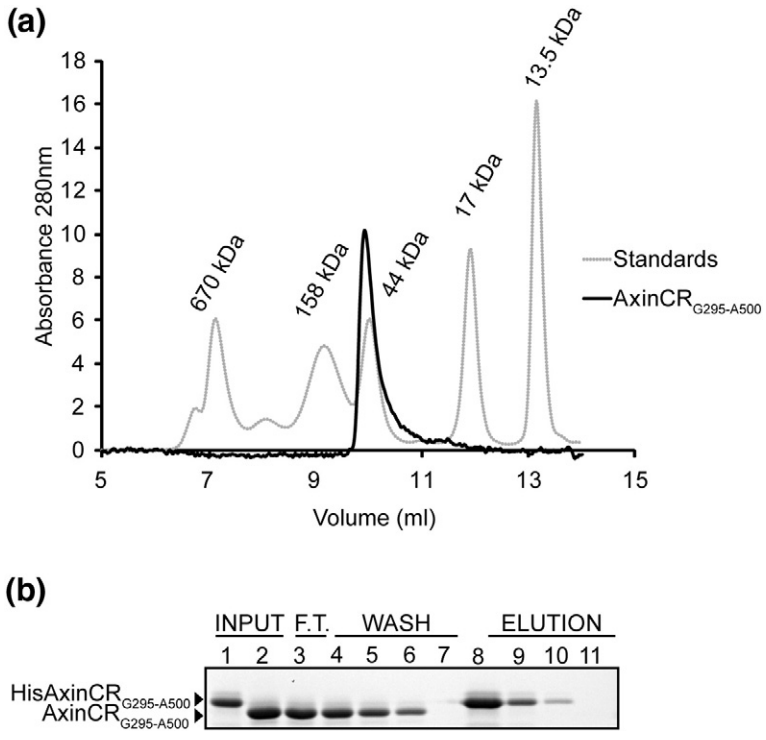

Fig. 4. AxinCR$_{G295\text{-}A500}$ displays an extended structure. (a) AxinCR$_{G295\text{-}A500}$ was applied on a Bio-Silect SEC analytical column. The elution volume of AxinCR$_{G295\text{-}A500}$ is 9.92 ml and corresponds to a molecular mass of 70 kDa, which is approximately three times the calculated molecular mass of 23 kDa. (b) AxinCR$_{G295\text{-}A500}$ does not self-interact. Purified His-tagged AxinCR$_{G295\text{-}A500}$ (lane 1; input) was incubated with untagged AxinCR$_{G295\text{-}A500}$ (lane 2; input). Subsequently, His-tagged AxinCR$_{G295\text{-}A500}$ was isolated with Ni-NTA beads in a pull-down assay. AxinCR$_{G295\text{-}A500}$ was abundantly detected in unbound wash fractions but did not coelute with His-tagged AxinCR$_{G295\text{-}A500}$ (lanes 8–10), indicating a lack of self-association.

that is significantly higher than the calculated mass of 23 kDa based on the primary amino acid sequence. The large apparent size of AxinCR$_{G295\text{-}A500}$ during size-exclusion chromatography could be attributed to either an unfolded extended shape or oligomerization. To exclude the latter possibility, we analyzed whether His-tagged AxinCR$_{G295\text{-}A500}$ could bind the untagged form by utilizing a pull-down assay. We could not detect any interaction between the two AxinCR$_{G295\text{-}A500}$ forms (Fig. 4b). These findings rule out the possibility that AxinCR$_{G295\text{-}A500}$ forms oligomers and support the assumption that AxinCR$_{G295\text{-}A500}$ bears an extended conformation lacking a hydrophobic core.

AxinCR$_{G295\text{-}A500}$ exhibits a random-coil secondary structure with residual helical elements

Next, we applied circular dichroism (CD) to gain insight into the presence of secondary structural elements in AxinCR$_{G295\text{-}A500}$. The far-UV CD spectrum yielded a negative peak of ellipticity at 201 nm, a typical feature of random-coil structures[35] (Fig. 5). To uncover whether residual helical elements in the AxinCR$_{G295\text{-}A500}$ fragment could be induced, we titrated increasing amounts of 2,2,2-trifluoroethanol (TFE), a helix-stabilizing agent that only acts on proteins that carry residual unstable helical structures by strengthening local H-bond interactions.[36] Addition of TFE shifted the negative peak to 208 nm and induced another negative peak at 222 nm and a positive peak at 190 nm, yielding a spectrum of a protein with significant α-helical content (Fig. 5). With the use of CD deconvolution algorithms (DichroWeb[37]), the α-helical content of Axin is estimated to be 21% under physiological conditions and increases to 58% under conditions of 20% TFE. These results indicate that AxinCR$_{G295\text{-}A500}$ has the tendency to form α-helical elements that are stabilized by conditions favoring intramolecular interactions.

AxinCR is predicted to lack order

To gain insight into the localization of helical elements and the overall structural organization of AxinCR$_{G295\text{-}A500}$ (Fig. 6a), we utilized bioinformatic tools to predict secondary structure binding sites and disorder tendency. We submitted the AxinCR$_{G295\text{-}A500}$ protein sequence to eight publicly available servers that predict secondary structure based on the primary sequence and to seven servers that predict protein disorder, implementing 12 algorithms (Fig. 6c and d). The chosen algorithms for disorder prediction were based on different criteria (reviewed by Ferron *et al.*[38]).

Individual prediction programs for secondary structure consistently predict three helical regions, two of which overlap with α-helical peptides previously cocrystallized in complex with GSK3β and β-catenin, respectively (Fig. 6c and d).[32,33] In contrast, the predicted extent of disordered regions is inconsistent, differing significantly between algorithms (Fig. 6d). Noticeably, the amino acid composition of AxinCR$_{G295\text{-}A500}$ reveals 52.8% disorder-

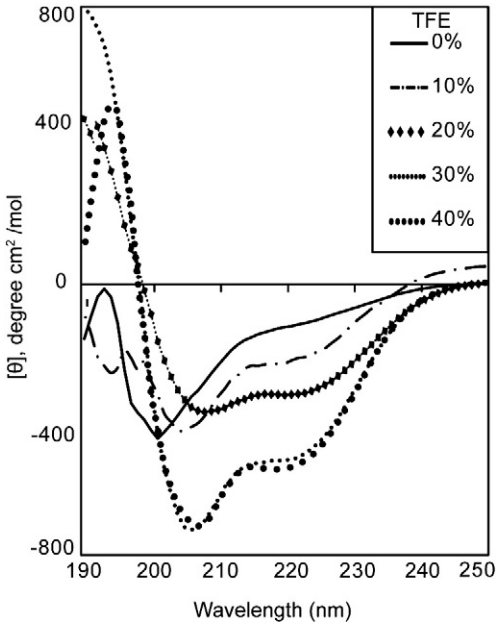

Fig. 5. AxinCR$_{G295\text{-}A500}$ displays a random-coil conformation with residual α-helical elements. Far-UV CD spectrum of AxinCR$_{G295\text{-}A500}$ in 10 mM phosphate buffer (pH 7.2), 50 mM NaF, and 0.5 mM TCEP. The spectra show a negative peak at 201 nm, which corresponds to a random-coil conformation. Titration of TFE induces a change in the spectrum, yielding negative peaks at 208 nm and 220 nm and a positive peak at 190 nm, characteristic of a protein containing α-helices.

promoting residues (D, M, K, R, S, Q, P, and E) and 33.7% order-promoting residues (C, W, Y, I, F, V, L, H, T, and N); in comparison, for the folded RGS domain, the respective fractions compose 44.4% and 45.2%.[39] Together with our experimental data, these predictions argue that AxinCR is unfolded while containing three short helices, which might only be stabilized by cofactors in the cell. As two of these helices perform protein–protein interactions and do not contain hydrophobic patches on their surface, we consider it unlikely for the three helical modules to form a hydrophobic core.

^{1}H–^{15}N heteronuclear single-quantum coherence NMR spectrum of AxinCR$_{G295\text{-}A500}$ reveals an unstructured conformation

To gain insight into the tertiary structure of AxinCR, we performed two-dimensional ^{1}H–^{15}N heteronuclear single-quantum coherence (HSQC) NMR analysis (Fig. 7). The resulting HSQC spectrum showed strongly clustered resonances in a narrow range of 7.6–8.6 ppm, which is characteristic of unfolded proteins.[40] To compare the properties of AxinCR$_{G295\text{-}A500}$ in physiological buffer with an entirely unfolded AxinCR$_{G295\text{-}A500}$, we repeated the two-dimensional ^{1}H–^{15}N HSQC NMR experiment in the presence of the denaturing agent urea. Both spectra reveal only minor differences, which most likely are caused by an increase in buffer viscosity upon addition of 5 M urea.[41] These results confirm that AxinCR$_{G295\text{-}A500}$ is intrinsically disordered under physiological conditions.

AxinCR$_{G295\text{-}A500}$ strongly enhances the GSK3β-mediated phosphorylation of β-catenin

To address the scaffolding role of AxinCR$_{G295\text{-}A500}$, we incubated GSK3β with a fixed amount of β-catenin substrate and titrated purified AxinCR$_{G295\text{-}A500}$ in this reaction. Titration of AxinCR$_{G295\text{-}A500}$ strongly enhanced the efficiency of GSK3β in phosphorylating β-catenin *in vitro* (Fig. 8a), whereas no effect was observed on AxinCR variants lacking either the β-catenin binding site (AxinCR$_{\Delta\beta cat}$) or the GSK3β binding site (AxinCR$_{\Delta GSK3\beta}$), suggesting that Axin binding of both GSK3β and β-catenin is required for its scaffolding function (Fig. 8b and c). Phosphorylation of the AxinCR$_{G295\text{-}A500}$ and AxinCR$_{\Delta\beta cat}$ fragments occurs equally well (Fig. 8a and b), suggesting that both variants adequately bind GSK3β. In contrast, AxinCR$_{\Delta GSK3\beta}$ remains largely unphosphorylated (Fig. 8c), confirming a lack of GSK3β binding. Quantification of β-catenin phosphorylation levels in these experiments demonstrates that the enhancement of β-catenin phosphorylation reaches a plateau and drops upon further titration of AxinCR$_{G295\text{-}A500}$ (Fig. 8d). These findings suggest the need for the formation of a trimolecular complex to most efficiently achieve β-catenin phosphorylation. AxinCR$_{G295\text{-}A500}$ excess likely titrates GSK3β away from β-catenin, thereby diminishing the efficiency of phosphorylation (Fig. 8e). We conclude that the highly flexible AxinCR$_{G295\text{-}A500}$ fragment scaffolds and targets GSK3β kinase activity towards its substrate, β-catenin.

Discussion

The tumor-suppressor protein Axin plays a crucial role in the control of Wnt signaling by coordinating the formation of a multiprotein complex that mediates the phosphorylation of the transcriptional regulator β-catenin.[4] The N-terminal RGS domain and the C-terminal DIX domain assist in the assembly of the complex by binding the scaffolding protein APC and by mediating Axin oligomerization, respectively, whereas AxinCR brings together the kinases CK1 and GSK3β and their substrate, β-catenin.[4] The structures of the RGS and DIX domains were solved previously,[26,31] but as of yet, the tertiary structure of the connecting and functionally important middle part of Axin has just been predicted to be disordered[42] and has not adequately been addressed.

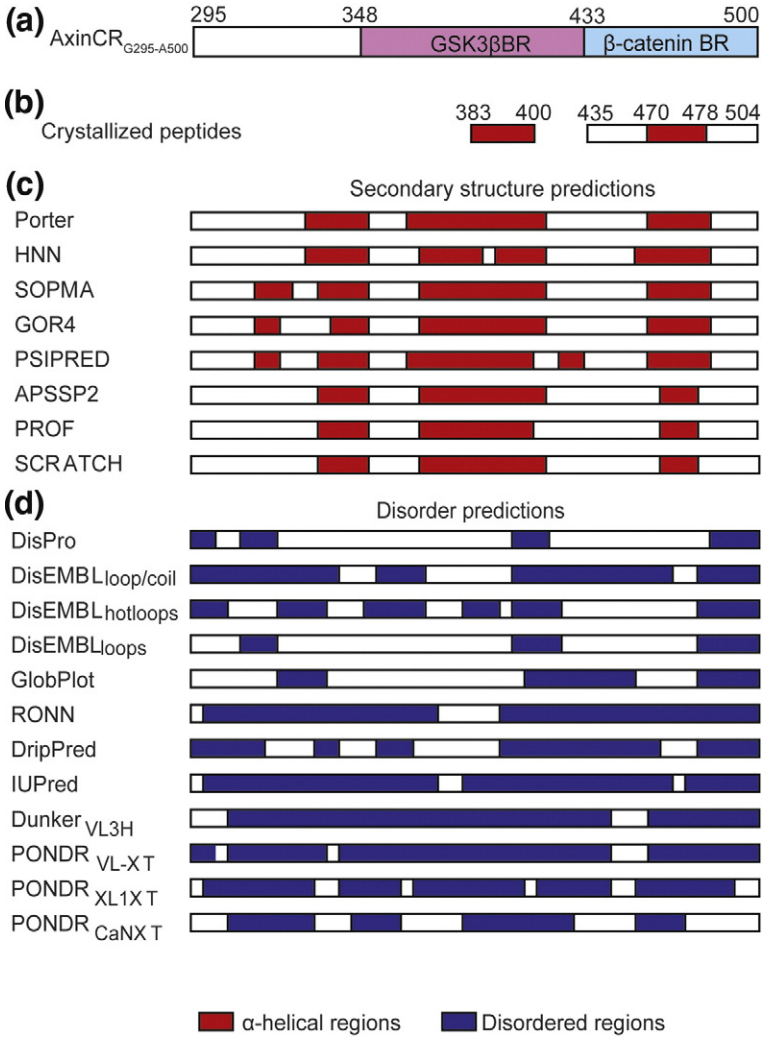

Fig. 6. Schematic representation of the structural characteristics of $AxinCR_{G295\text{-}A500}$. (a) Schematic representation of $AxinCR_{G295\text{-}A500}$. (b) Schematic representation of the two α-helical Axin peptides cocrystallized with GSK3β[32] and β-catenin.[33] (c) Secondary structure predictions for $AxinCR_{G295\text{-}A500}$ were performed using eight algorithms in publicly available servers. Bars represent the predicted secondary structure elements of different algorithms. Segments that are predicted to be α-helical are indicated in red. (d) Disorder predictions for $AxinCR_{G295\text{-}A500}$ were performed using 12 algorithms in publicly available servers. Bars represent predicted disorder according to different algorithms, as indicated. Segments that are predicted to be disordered are depicted in blue.

Here, we have used a variety of biophysical and biochemical techniques to analyze the conformation of AxinCR. Our results convincingly show that the large AxinCR is intrinsically disordered under physiological conditions. Despite the clear lack of rigid tertiary structure in AxinCR, residual helical elements may be present, as shown by CD analysis. The unstable interconverting helical elements are stabilized by conditions that favor intramolecular hydrogen-bond formation (Fig. 5). In accordance with these findings, two independent AxinCR peptides that were cocrystallized with GSK3β[32] and β-catenin[33] showed α-helical conformation. Together, these results argue that residual helical regions in unbound AxinCR may be stabilized with their interaction partners during complex formation. Indeed, disorder-to-order transitions that accompany the molecular recognition of disordered proteins are reported in an increasing number of cases.[39,42–44] The rudimentary presence of helices in the conformational equilibrium would also allow recruitment of partner proteins via conformational selection.[45]

How does the large intrinsically disordered region facilitate the multiple roles of Axin in different and crucial developmental signaling pathways? Besides mediating β-catenin phosphorylation, the middle part of Axin accommodates multiple additional protein–protein interactions, the majority of which act in important signaling pathways [e.g., transforming growth factor β, c-Jun N-terminal kinase (JNK), and p53][46–51] (Fig. 9). Several of the binding sites of these interaction partners overlap. It remains unresolved how Axin, typified as the limiting component of the β-catenin destruction complex,[52] may serve various functions in the cell. To meet this requirement, the intrinsically disordered propensity of AxinCR would provide a highly flexible and extended surface for interactions of low affinity and high specificity[42] (Fig. 9). As a consequence, implicated protein interactions are fast and transient. For specificity to be secured, selective induction of (partial) folding or secondary structure formation by interacting proteins may serve to shape the conformation of the disordered region to

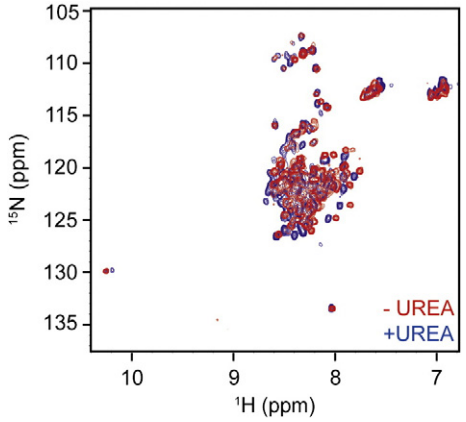

Fig. 7. AxinCR$_{G295\text{-}A500}$ is predominantly unfolded. The ^{1}H–^{15}N HSQC spectrum of AxinCR$_{G295\text{-}A500}$ in 10 mM phosphate buffer (pH 7.2) with anionic-strength 300 mM NaCl, 0.5 mM TCEP, 10% D_2O, and 2.5% DSS is represented in red. The fingerprint resonance from amide protons of peptide bonds is not well dispersed and ranges from 7.6 ppm to 8.5 ppm, reflecting an unstructured conformation. The ^{1}H–^{15}N HSQC spectrum of AxinCR$_{G295\text{-}A500}$ in 10 mM phosphate buffer (pH 7.2) with 300 mM NaCl, 0.5 mM TCEP, 10% D_2O, 2.5% DSS, and 5 M urea is represented in blue. The two spectra show significant overlap, indicating a lack of structure of AxinCR under physiological conditions.

the needs of one single signaling pathway at the time.[39,42–44] Hence, folding of disordered regions by the binding of one binding partner at "site A" would allosterically couple to the binding events of another factor at "site B" (site-to-site communication).[53] In agreement with this hypothesis, two JNK pathway factors, MEKK1 and MEKK4, compete for binding to Axin, whereas their binding sites are located in separate nonoverlapping regions in the unstructured middle part of Axin.[54]

The role of AxinCR in the Wnt pathway is to bring the GSK3β kinase and its substrate, β-catenin, in close proximity, thereby catalyzing the phosphorylation of the flexible β-catenin N-terminal tail. Hence, Axin forces specificity on the broadly involved GSK3β kinase to phosphorylate β-catenin. Interestingly, the repeat regions in APC that bind Axin and β-catenin are located in a predicted natively disordered region as well.[55] The corresponding transient nature of multiple protein–protein interactions in the complex would allow a rapid handover of the β-catenin substrate from Axin to APC, from APC to the E3 ligase β-transducin repeat-containing protein, and, finally, to the proteasome.[3] Of note, other functionally important binding partners of β-catenin (e.g., E-cadherin and Tcf) interact through extended unfolded protein segments as well, suggesting the importance of disordered domains in the regulation of a key signaling pathway protein.[56]

Mutations in Axin are strongly linked to the development of cancer.[18,19,57] Many missense mutations, as reported in colorectal carcinoma, medulloblastoma, and hepatocellular carcinoma, hit AxinCR[18,19] (Fig. 1). Inhibition or downregulation of the tumor-suppressor protein Axin is believed to contribute to tumor formation.[18] Regarding the lack of structure of AxinCR, missense mutations are unlikely to affect protein function and stability by misfolding, but rather would interfere with the binding of partner proteins to linear motifs, or may disturb interaction due to conformational selection. Remarkably, however, many of these mutations affect residues outside the linear binding motifs for β-catenin and GSK3β. How these mutations deregulate GSK3β activity towards β-catenin remains the subject of further studies.

In summary, we demonstrate that the functionally important AxinCR is natively unfolded under physiological conditions. These findings bear importance for our current study of the mechanism by which Axin performs its tumor-suppressor function.

Materials and Methods

Construct generation and protein expression

The fragments encompassing the central regions of human Axin1, AxinCR$_{G295\text{-}A500}$, AxinCR$_{\Delta\beta cat}$ (G295-G430), and AxinCR$_{\Delta GSK3\beta}$ (G433-V600), as well as the RGS domains of Axin (N2-V220), human β-catenin (full length and N138-L781), and human GSK3β, were amplified by PCR. All AxinCR fragments were cloned in the bacterial expression vector pET-24a(+) (Novagen). pET-24a(+) was modified by insertion of a six-histidine tag and a tobacco etch virus (TEV) protease cleavage site (between NdeI and EcoRI) to provide a cleavable tag at the N-terminus of the fused protein. GSK3β, β-catenin, and AxinRGS were cloned in pET-50b(+) (Novagen). All proteins were expressed in *Escherichia coli* Rosetta2 cells (Merck4Biosciences).

Cells expressing Axin fragments were grown in Luria–Bertani medium. M9 minimal medium enriched with $^{15}NH_4Cl$ (Cambridge Isotope Laboratories, Inc.) was used for NMR purposes. At the time point where the optical density (OD_{600}) had reached 0.6, protein expression was induced by addition of 0.5 mM isopropyl β-D-1-thiogalactopyranoside (Roche). Bacterial cultures expressing all AxinCR fragments and β-catenin$_{N138\text{-}L781}$ were incubated at 20 °C for 4 h, and cultures expressing AxinRGS were incubated at 18 °C for 16 h.

Cells transformed with the β-catenin and GSK3β constructs were grown in Terrific broth autoinduction medium at 30 °C. At the time point where the OD_{600} had reached 3, the temperature was decreased to 15 °C, and the cells grew until the OD_{600} had reached 15.

Protein purification

Bacterial Rosetta cells expressing Axin fragments and β-catenin$_{N138\text{-}L781}$ were pelleted, resuspended in buffer A

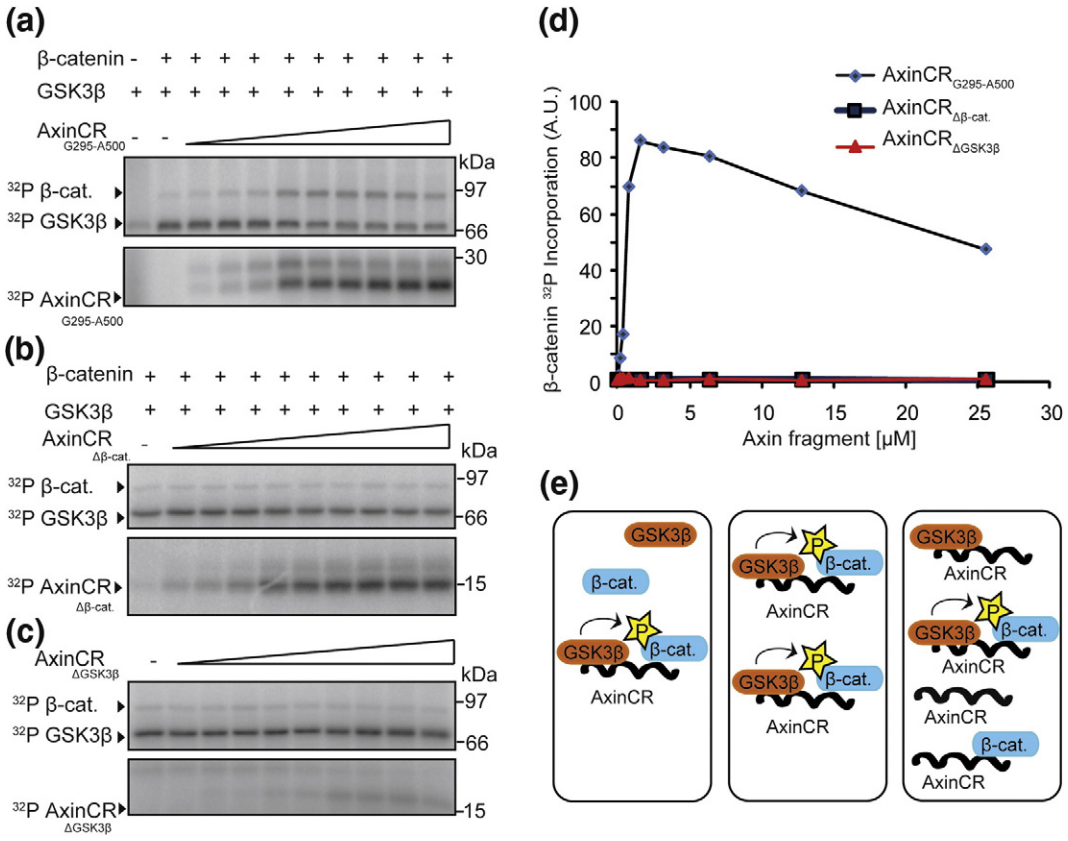

Fig. 8. AxinCR$_{G295\text{-}A500}$ facilitates the phosphorylation of β-catenin. *In vitro* phosphorylation of β-catenin by GSK3β in the absence and in the presence of a titration series of (a) AxinCR$_{G295\text{-}A500}$, (b) AxinCR$_{\Delta\beta cat}$, and (c) AxinCR$_{\Delta GSK3\beta}$. The phosphorylation of Axin fragments is also shown. (d) Quantification of the ^{32}P incorporation of β-catenin for all reactions (a–c). The intensities were normalized against the value of the phosphorylated β-catenin in the absence of the Axin fragment. (e) Model depicting the effects of low (left), moderate (middle), and high (right) abundances of AxinCR$_{G295\text{-}A500}$ on GSK3β-mediated kinase activity towards β-catenin. Under optimal stoichiometric conditions (middle), the majority of molecules are involved in trimolecular complex formation, providing the maximal phosphorylation of β-catenin. AxinCR excess (right) inhibits the formation of complexes composed of all three proteins, leading to a decrease in phosphorylation efficiency.

[50 mM Tris–HCl (pH 7.5), 300 mM NaCl, 20 mM imidazole, 0.5 mM tris(2-carboxyethyl)phosphine (TCEP), and Complete Protease Inhibitor Cocktail EDTA-Free Tablets (Roche)], and lysed by sonication (Sonifier B12; Branson Ultrasonic). A subsequent ultracentrifugation step (30,000 rpm for 45 min at 4 °C) separated the soluble proteins from the insoluble proteins. The soluble fraction was filtered and applied to a POROS 20MC column (metal-chelate affinity chromatography; Applied Biosystems) connected to an Äkta Purifier chromatography system (GE Healthcare). The column was equilibrated with 10 column volumes (CV) of buffer A, and a linear gradient between and buffer A and buffer B [50 mM Tris–HCl (pH 7.5), 300 mM NaCl, 1 M imidazole, and 0.5 mM TCEP] was applied to elute His-tagged proteins. Fractions were collected and analyzed by SDS-PAGE. Appropriate fractions containing His-tagged proteins were applied to a HiTrap desalting column (GE Healthcare) to exchange buffer B with 50 mM Tris–HCl (pH 7.5), 150 mM NaCl, and 0.5 mM TCEP. Recombinant His-tagged TEV protease, which was modified to enhance stability (L56V/S135G; the expression construct was a kind gift of Cabrita *et al.*[58]), was added at a His-tagged protein/TEV ratio of 8:1. Cleavage took place at 37 °C for 3 h in the presence of 1 mM dithiothreitol (DTT). Next, the cleaved AxinCR$_{G295\text{-}A500}$, AxinCR$_{\Delta\beta cat}$, and AxinRGS proteins were further purified by anion-exchange chromatography after a decrease of the salt concentration to 30 mM NaCl. A segmented gradient between equilibration buffer [50 mM Tris–HCl (pH 9) and 0.5 mM TCEP] and elution buffer [50 mM Tris–HCl (pH 9), 1 M NaCl, and 0.5 mM TCEP] eluted Axin fragments with 95% purity, as determined by SDS-PAGE and Coomassie brilliant blue G-250 (Serva) staining. AxinCR$_{\Delta GSK3\beta}$ was separated by the TEV protease using a second affinity purification.

Bacterial cells expressing GSK3β and β-catenin were pelleted, resuspended in buffer C [50 mM Tris–HCl (pH 7.5), 500 mM NaCl, 1 mM TCEP, 10% glycerol, and Complete Protease Inhibitor Cocktail EDTA-Free Tablets (Roche)], and lysed mechanically by two passages through a cell cracker (EmulsiFlex-C5; Avestin). The lysate was cleared from aggregates at 45,000*g* for 50 min, and the supernatant was filtered and loaded on a POROS 20MC column. The column was equilibrated with 10 CV of

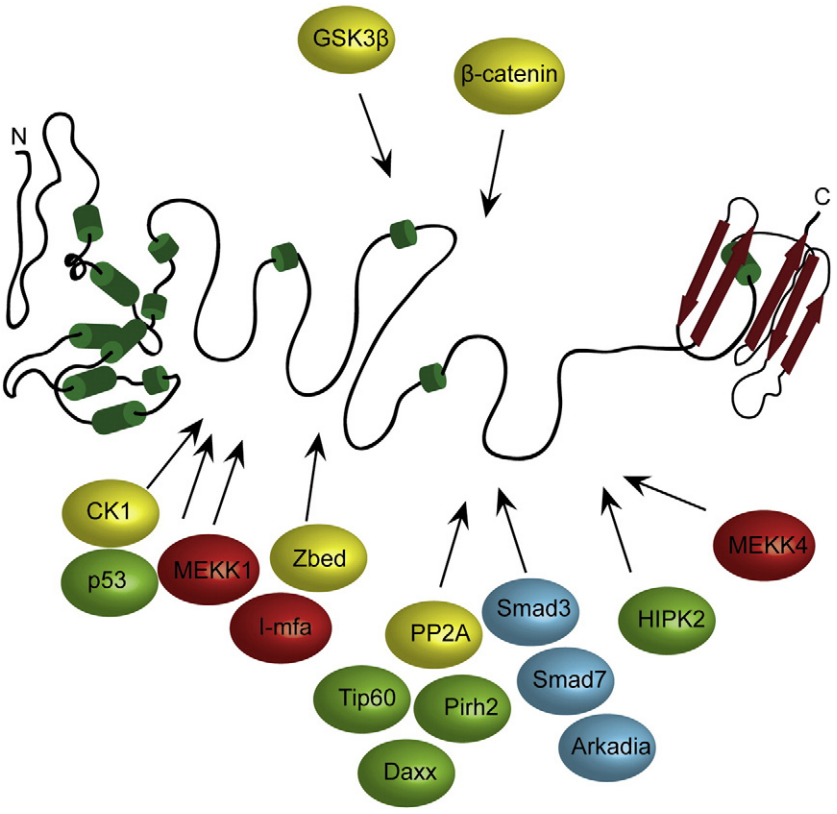

Fig. 9. Model of Axin as a highly flexible scaffolding protein in multiple signaling pathways. AxinCR contains overlapping binding sites for multiple proteins acting in key signaling pathways. Proteins that act simultaneously through their interaction with Axin in the Wnt (yellow), transforming growth factor β (blue), JNK (red), and p53 (green) pathways are indicated.

buffer C, and a linear gradient between buffer C and buffer D [50 mM Tris–HCl (pH 7.5), 500 mM NaCl, 1 mM TCEP, 10% glycerol, and 1 M imidazole] was applied to elute His-tagged proteins.

Interaction assays

Purified $AxinCR_{G295\text{-}A500}$ was pulled down via affinity chromatography using purified His-NusA-GSK3β or His-β-catenin. His-NusA was used as negative control to verify the specificity of the interaction. His-$AxinCR_{G295\text{-}A500}$ was used in order to examine the possibility of $AxinCR_{G295\text{-}A500}$ self-interaction. In all assays, $AxinCR_{G295\text{-}A500}$ was incubated with each His tagged protein for 2 h at 4 °C. Samples were loaded on gravity flow columns (Bio-Rad) with Ni^{2+} beads (Qiagen) equilibrated in buffer F [50 mM Tris–HCl (pH 7.5), 100 mM NaCl, 20 mM imidazole, and 1 mM TCEP] and incubated for 1 h at 4 °C. Through gravity flow, unbound proteins were removed, and the beads were washed with 10 CV of buffer F. Bound protein complexes were eluted with 4 CV of buffer G [50 mM Tris–HCl (pH 7.5), 100 mM NaCl, 500 mM imidazole, and 1 mM TCEP]. Samples were taken from all steps and analyzed on SDS-PAGE.

HEK293T cells were transfected with pEBG-2T (a mammalian GST expression vector) with or without $AxinCR_{G295\text{-}A500}$ as fused protein. Cells were lysed in lysis buffer [50 mM Tris–HCl (pH 7.5), 100 mM NaCl, 50 mM NaF, 1% Triton, 1 mM DTT, 1 mM Na_3VO_4, and protease inhibitors] at 4 °C. The soluble proteins were separated from cell debris via centrifugation and incubated with preequilibrated Glutathione Sepharose™ 4B bead (GS-4B) slurry (GE Healthcare) for 2 h at 4 °C. The beads were extensively washed with lysis buffer to eliminate aspecific binding. GST fusion protein complexes were eluted from the GS-4B beads with SDS sample buffer and denaturation (105 °C for 5 min). Samples were taken from all steps and analyzed by Western blot analysis.

Antibodies and siRNA

This study used mouse anti-GST antibody (Abcam), mouse anti-β-catenin antibody (BD Transduction Laboratories), rabbit anti-GSK3β antibody (Cell Signaling Technology), goat anti-Axin antibody (R&D Systems), mouse–anti-tubulin antibody (Sigma), and control siRNA and siRNA against β-catenin (Ambion).

Silencing of β-catenin

Cells were transfected with 64 nM control siRNA or siRNA against β-catenin. Transfection was performed using Lipofectamine 2000 in accordance with the manufacturer's instructions. Forty eight hours after transfection, cells were lysed and β-catenin levels were analyzed by Western blot analysis.

Mammalian expression constructs and reporter assay

Human $AxinCR_{G295\text{-}A500}$ was subcloned into a GST mammalian expression vector (pEBG-2T), and full-length

GST-tagged Axin was subcloned into pCS2. As mock, we used pEBG-2T without any fused protein. HEK293T cells were seeded in 24-well plates and cotransfected in duplicate with 100 ng of the indicated Axin constructs and 30 ng of the luciferase reporter construct TOPflash or FOPflash.[34] Transfection efficiency in luciferase reporter assays was controlled and normalized by including a constant amount of TK Renilla reporter plasmid in all transfections. At 24 h after transfection, cells were treated with WCM or control L-cell medium for 16 h. Cells were lysed in passive lysis buffer (Promega), and luciferase activities were measured with the dual-luciferase reporter assay system (Promega) in accordance with the manufacturer's instructions.

Fluorometric analysis

Purified $AxinCR_{G295\text{-}A500}$ (10 μM) or AxinRGS (10 μM) in 10 mM sodium phosphate (pH 7.2), 150 mM NaCl, and 1 mM DTT was measured on a spectrophotometer (Perkin-Elmer LS55) with a 1.5-ml cuvette (Hellma) with a magnetic stirrer using the software Fluo_pe (D. Veprintsev; LMB Cambridge, UK). Fluorometric analysis was performed at increasing temperatures ranging from 20.1 °C to 80.1 °C for $AxinCR_{G295\text{-}A500}$ and from 21.4 °C to 72.7 °C for AxinCR, with a 1 °C step increase. Fluorescence was measured with excitation at 280 nm and with emission at a range from 300 nm to 400 nm.

Analytical gel filtration

Analytical gel filtration of purified $AxinCR_{G295\text{-}A500}$ at a concentration of 500 μM was performed on an Äkta Purifier (GE Healthcare) using a Bio-Silect SEC250 analytical column (300 mm × 7.8 mm) with a guard column (50 mm × 7.8 mm; Bio-Rad) equilibrated with 25 mM Tris–HCl (pH 7.2), 150 mM NaCl, and 1 mM TCEP. AxinCR was eluted at a flow rate of 1 ml/min, and the elution profile was recorded by continuously monitoring UV absorbance at 280 nm and 220 nm. The calibration curve was made using molecular mass standards from a lyophilized protein test mix (Bio-Rad), including thyroglobulin (670 kDa), γ globulin (158 kDa), ovalbumin (44 kDa), myoglobin (17 kDa), and vitamin B_{12} (1.3 kDa).

Circular dichroism

CD spectra were recorded with a J-810 spectropolarimeter (Jasco). Purified $AxinCR_{G295\text{-}A500}$ (40 μM) in 10 mM sodium phosphate (pH 7.2), 50 mM NaF, and 0.5 mM TCEP was applied on a 1-mm Quartz cell (Hellma). Far-UV spectra were collected over a range of 190–260 nm using Jasco software at a scanning speed of 50 nm/min and at a data pitch of 1 nm, averaged over 10 acquisitions. Spectra were corrected for buffer contributions. Different concentrations of TFE were used: 10%, 20%, 30%, and 40% (vol/vol).

Disorder and secondary structure predictions

The primary protein sequence of AxinCR from Gly295 to Ala500 (GenBank accession number AAH44648.1) was submitted to seven publicly available servers implementing 12 different algorithms for protein disorder prediction. Eight publicly available algorithms were used for secondary structure predictions. In all cases, we used the default parameters. The servers used are as follows: SCRATCH/DisPro,[59] DisEMBL,[60] GlobPlot,[61] RONN,[62] DripPrep, IUPred,[63] PONDOR,[64] Porter,[65] HNN, SORMA, GOR4,[66] PSIPRED,[67] APSSP2, and PROF.[68]

NMR spectroscopy

^{15}N–^{1}H HSQC experiment was performed using 0.6 mM purified ^{15}N-labeled $AxinCR_{G295\text{-}A500}$ in buffer E [10 mM phosphate buffer (pH 7.2), 300 mM NaCl, 0.5 mM TCEP, 10% D_2O, and 2.5% 2,2-dimethyl-2-silapentane-5-sulfonate (DSS)] and in buffer E plus 5 M urea. Spectra were measured at 25 °C on a Bruker DRX600 instrument equipped with a TCI cryoprobe. Spectra were processed with Topspin (Bruker) and analyzed with SPARKY software (T. D. Goddard and D. G. Keller, SPARKY 3, University of California, San Francisco).

In vitro phosphorylation

GSK3 (7 nM; BioVision) was added to phosphorylation buffer [50 mM Tris–HCl (pH 7.5), 100 mM NaCl, 10 mM $MgCl_2$, 1 mM DTT, and 10 μCi of [γ-^{32}P]ATP (3000 Ci/mmol)] to phosphorylate 1 μM recombinant β-catenin in a of total volume of 30 μl. Samples were incubated at 30 °C for 45 min in the absence or in the presence of purified $AxinCR_{G295\text{-}A500}$, $AxinCR_{\Delta\beta cat}$ (G295-G430), and $AxinCR\text{-}_{\Delta GSK3\beta}$ (G433-V600) (0.1 μM, 0.2 μM, 0.4 μM, 0.8 μM, 1.6 μM, 3.2 μM, 6.4 μM, 12.8 μM, and 25.6 μM). Samples were mixed with SDS sample buffer and loaded on gels. The gels were dried, and a phospho imager screen (Molecular Dynamics) was used to measure radioactivity with the Storm scanner (Amersham Biosciences). The intensities were quantified by ImageQuant software (Molecular Dynamics).

Acknowledgements

This work was supported by the Dutch Cancer Society (UU 2006-3508), the European Research Council (European Research Council starting grant 242958 to M.M.M.), the Utrecht University (High Potential Grants to M.M.M. and S.G.D.R.), the European Union (Marie-Curie-Excellence Grant to S.G.D.R.), and the Netherlands Organization for Scientific Research NWO (VIDI career development grant to S.G.D.R.). A.F. was supported by European Research Council starting grant 203413. We thank Jacques P. F. Doux and Tania Rutters-Meijneke (Biochemistry of Membranes, Bijvoet Center) for help with CD experiments.

Supplementary Data

Supplementary data associated with this article can be found, in the online version, at doi:10.1016/j.jmb.2010.11.013

References

1. Logan, C. Y. & Nusse, R. (2004). The Wnt signaling pathway in development and disease. *Annu. Rev. Cell Dev. Biol.* **20**, 781–810.
2. Clevers, H. (2006). Wnt/beta-catenin signaling in development and disease. *Cell*, **127**, 469–480.
3. MacDonald, B. T., Tamai, K. & He, X. (2009). Wnt/beta-catenin signaling: components, mechanisms, and diseases. *Dev. Cell*, **17**, 9–26.
4. Kimelman, D. & Xu, W. (2006). Beta-catenin destruction complex: insights and questions from a structural perspective. *Oncogene*, **25**, 7482–7491.
5. Ikeda, S., Kishida, S., Yamamoto, H., Murai, H., Koyama, S. & Kikuchi, A. (1998). Axin, a negative regulator of the Wnt signaling pathway, forms a complex with GSK-3beta and beta-catenin and promotes GSK-3beta-dependent phosphorylation of beta-catenin. *EMBO J.* **17**, 1371–1384.
6. Sakanaka, C., Weiss, J. B. & Williams, L. T. (1998). Bridging of beta-catenin and glycogen synthase kinase-3beta by axin and inhibition of beta-catenin-mediated transcription. *Proc. Natl Acad. Sci. USA*, **95**, 3020–3023.
7. Itoh, K., Krupnik, V. E. & Sokol, S. Y. (1998). Axis determination in *Xenopus* involves biochemical interactions of axin, glycogen synthase kinase 3 and beta-catenin. *Curr. Biol.* **8**, 591–594.
8. Hart, M. J., de los Santos, R., Albert, I. N., Rubinfeld, B. & Polakis, P. (1998). Downregulation of beta-catenin by human Axin and its association with the APC tumor suppressor, beta-catenin and GSK3 beta. *Curr. Biol.* **8**, 573–581.
9. Aberle, H., Bauer, A., Stappert, J., Kispert, A. & Kemler, R. (1997). Beta-catenin is a target for the ubiquitin–proteasome pathway. *EMBO J.* **16**, 3797–3804.
10. Liu, C., Li, Y., Semenov, M., Han, C., Baeg, G. H., Tan, Y. *et al.* (2002). Control of beta-catenin phosphorylation/degradation by a dual-kinase mechanism. *Cell*, **108**, 837–847.
11. Orford, K., Crockett, C., Jensen, J. P., Weissman, A. M. & Byers, S. W. (1997). Serine phosphorylation-regulated ubiquitination and degradation of beta-catenin. *J. Biol. Chem.* **272**, 24735–24738.
12. Peifer, M., Pai, L. M. & Casey, M. (1994). Phosphorylation of the *Drosophila* adherens junction protein Armadillo: roles for wingless signal and zeste-white 3 kinase. *Dev. Biol.* **166**, 543–556.
13. van Noort, M., Meeldijk, J., van der Zee, R., Destree, O. & Clevers, H. (2002). Wnt signaling controls the phosphorylation status of beta-catenin. *J. Biol. Chem.* **277**, 17901–17905.
14. Amit, S., Hatzubai, A., Birman, Y., Andersen, J. S., Ben-Shushan, E., Mann, M. *et al.* (2002). Axin-mediated CKI phosphorylation of beta-catenin at Ser 45: a molecular switch for the Wnt pathway. *Genes Dev.* **16**, 1066–1076.
15. Yanagawa, S., Matsuda, Y., Lee, J. S., Matsubayashi, H., Sese, S., Kadowaki, T. & Ishimoto, A. (2002). Casein kinase I phosphorylates the Armadillo protein and induces its degradation in *Drosophila*. *EMBO J.* **21**, 1733–1742.
16. Davidson, G., Wu, W., Shen, J., Bilic, J., Fenger, U., Stannek, P. *et al.* (2005). Casein kinase 1 gamma couples Wnt receptor activation to cytoplasmic signal transduction. *Nature*, **438**, 867–872.
17. Zeng, X., Tamai, K., Doble, B., Li, S., Huang, H., Habas, R. *et al.* (2005). A dual-kinase mechanism for Wnt co-receptor phosphorylation and activation. *Nature*, **438**, 873–877.
18. Salahshor, S. & Woodgett, J. R. (2005). The links between axin and carcinogenesis. *J. Clin. Pathol.* **58**, 225–236.
19. Kim, Y. D., Park, C. H., Kim, H. S., Choi, S. K., Rew, J. S., Kim, D. Y. *et al.* (2008). Genetic alterations of Wnt signaling pathway-associated genes in hepatocellular carcinoma. *J. Gastroenterol. Hepatol.* **23**, 110–118.
20. Fearnhead, N. S., Wilding, J. L., Winney, B., Tonks, S., Bartlett, S., Bicknell, D. C. *et al.* (2004). Multiple rare variants in different genes account for multifactorial inherited susceptibility to colorectal adenomas. *Proc. Natl Acad. Sci. USA*, **101**, 15992–15997.
21. Sarrio, D., Moreno-Bueno, G., Sanchez-Estevez, C., Banon-Rodriguez, I., Hernandez-Cortes, G., Hardisson, D. & Palacios, J. (2006). Expression of cadherins and catenins correlates with distinct histologic types of ovarian carcinomas. *Hum. Pathol.* **37**, 1042–1049.
22. Dahmen, R. P., Koch, A., Denkhaus, D., Tonn, J. C., Sorensen, N., Berthold, F. *et al.* (2001). Deletions of AXIN1, a component of the WNT/wingless pathway, in sporadic medulloblastomas. *Cancer Res.* **61**, 7039–7043.
23. McCartney, B. M. & Nathke, I. S. (2008). Cell regulation by the APC protein Apc as master regulator of epithelia. *Curr. Opin. Cell Biol.* **20**, 186–193.
24. Kishida, S., Yamamoto, H., Hino, S., Ikeda, S., Kishida, M. & Kikuchi, A. (1999). DIX domains of Dvl and axin are necessary for protein interactions and their ability to regulate beta-catenin stability. *Mol. Cell. Biol.* **19**, 4414–4422.
25. Sakanaka, C. & Williams, L. T. (1999). Functional domains of axin. Importance of the C terminus as an oligomerization domain. *J. Biol. Chem.* **274**, 14090–14093.
26. Schwarz-Romond, T., Fiedler, M., Shibata, N., Butler, P. J., Kikuchi, A., Higuchi, Y. & Bienz, M. (2007). The DIX domain of Dishevelled confers Wnt signaling by dynamic polymerization. *Nat. Struct. Mol. Biol.* **14**, 484–492.
27. Kishida, S., Yamamoto, H., Ikeda, S., Kishida, M., Sakamoto, I., Koyama, S. & Kikuchi, A. (1998). Axin, a negative regulator of the Wnt signaling pathway, directly interacts with adenomatous polyposis coli and regulates the stabilization of beta-catenin. *J. Biol. Chem.* **273**, 10823–10826.
28. Hedgepeth, C. M., Deardorff, M. A., Rankin, K. & Klein, P. S. (1999). Regulation of glycogen synthase kinase 3beta and downstream Wnt signaling by axin. *Mol. Cell. Biol.* **19**, 7147–7157.
29. Hinoi, T., Yamamoto, H., Kishida, M., Takada, S., Kishida, S. & Kikuchi, A. (2000). Complex formation of adenomatous polyposis coli gene product and axin facilitates glycogen synthase kinase-3 beta-dependent phosphorylation of beta-catenin and down-regulates beta-catenin. *J. Biol. Chem.* **275**, 34399–34406.
30. Yamamoto, H., Kishida, S., Kishida, M., Ikeda, S., Takada, S. & Kikuchi, A. (1999). Phosphorylation of

axin, a Wnt signal negative regulator, by glycogen synthase kinase-3beta regulates its stability. *J. Biol. Chem.* **274**, 10681–10684.
31. Spink, K. E., Polakis, P. & Weis, W. I. (2000). Structural basis of the Axin–adenomatous polyposis coli interaction. *EMBO J.* **19**, 2270–2279.
32. Dajani, R., Fraser, E., Roe, S. M., Yeo, M., Good, V. M., Thompson, V. *et al.* (2003). Structural basis for recruitment of glycogen synthase kinase 3beta to the axin–APC scaffold complex. *EMBO J.* **22**, 494–501.
33. Xing, Y., Clements, W. K., Kimelman, D. & Xu, W. (2003). Crystal structure of a beta-catenin/axin complex suggests a mechanism for the beta-catenin destruction complex. *Genes Dev.* **17**, 2753–2764.
34. Korinek, V., Barker, N., Morin, P. J., van Wichen, D., de Weger, R., Kinzler, K. W. *et al.* (1997). Constitutive transcriptional activation by a beta-catenin–Tcf complex in $APC^{-/-}$ colon carcinoma. *Science*, **275**, 1784–1787.
35. Greenfield, N. J. (2006). Using circular dichroism spectra to estimate protein secondary structure. *Nat. Protoc.* **1**, 2876–2890.
36. Gast, K., Zirwer, D., Muller-Frohne, M. & Damaschun, G. (1999). Trifluoroethanol-induced conformational transitions of proteins: insights gained from the differences between alpha-lactalbumin and ribonuclease A. *Protein Sci.* **8**, 625–634.
37. Whitmore, L. & Wallace, B. A. (2008). Protein secondary structure analyses from circular dichroism spectroscopy: methods and reference databases. *Biopolymers*, **89**, 392–400.
38. Ferron, F., Longhi, S., Canard, B. & Karlin, D. (2006). A practical overview of protein disorder prediction methods. *Proteins*, **65**, 1–14.
39. Dunker, A. K., Oldfield, C. J., Meng, J., Romero, P., Yang, J. Y., Chen, J. W. *et al.* (2008). The unfoldomics decade: an update on intrinsically disordered proteins. *BMC Genomics*, **9**, S1.
40. Libich, D. S., Monette, M. M., Robertson, V. J. & Harauz, G. (2007). NMR assignment of an intrinsically disordered protein under physiological conditions: the 18.5 kDa isoform of murine myelin basic protein. *Biomol. NMR Assign.* **1**, 61–63.
41. Kawahara, K. & Tanford, C. (1966). Viscosity and density of aqueous solutions of urea and guanidine hydrochloride. *J. Biol. Chem.* **241**, 3228–3232.
42. Cortese, M. S., Uversky, V. N. & Dunker, A. K. (2008). Intrinsic disorder in scaffold proteins: getting more from less. *Prog. Biophys. Mol. Biol.* **98**, 85–106.
43. Tompa, P. & Fuxreiter, M. (2008). Fuzzy complexes: polymorphism and structural disorder in protein–protein interactions. *Trends Biochem. Sci.* **33**, 2–8.
44. Sugase, K., Dyson, H. J. & Wright, P. E. (2007). Mechanism of coupled folding and binding of an intrinsically disordered protein. *Nature*, **447**, 1021–1025.
45. Boehr, D. D., Nussinov, R. & Wright, P. E. (2009). The role of dynamic conformational ensembles in biomolecular recognition. *Nat. Chem. Biol.* **5**, 789–796.
46. Luo, W. & Lin, S. C. (2004). Axin: a master scaffold for multiple signaling pathways. *Neurosignals*, **13**, 99–113.
47. Liu, W., Rui, H., Wang, J., Lin, S., He, Y., Chen, M. *et al.* (2006). Axin is a scaffold protein in TGF-beta signaling that promotes degradation of Smad7 by Arkadia. *EMBO J.* **25**, 1646–1658.
48. Guo, X., Ramirez, A., Waddell, D. S., Li, Z., Liu, X. & Wang, X. F. (2008). Axin and GSK3-control Smad3 protein stability and modulate TGF-signaling. *Genes Dev.* **22**, 106–120.
49. Rui, Y., Xu, Z., Lin, S., Li, Q., Rui, H., Luo, W. *et al.* (2004). Axin stimulates p53 functions by activation of HIPK2 kinase through multimeric complex formation. *EMBO J.* **23**, 4583–4594.
50. Li, Q., Wang, X., Wu, X., Rui, Y., Liu, W., Wang, J. *et al.* (2007). Daxx cooperates with the Axin/HIPK2/p53 complex to induce cell death. *Cancer Res.* **67**, 66–74.
51. Li, Q., Lin, S., Wang, X., Lian, G., Lu, Z., Guo, H. *et al.* (2009). Axin determines cell fate by controlling the p53 activation threshold after DNA damage. *Nat. Cell Biol.* **11**, 1128–1134.
52. Lee, E., Salic, A., Kruger, R., Heinrich, R. & Kirschner, M. W. (2003). The roles of APC and Axin derived from experimental and theoretical analysis of the Wnt pathway. *PLoS Biol.* **1**, E10.
53. Hilser, V. J. & Thompson, E. B. (2007). Intrinsic disorder as a mechanism to optimize allosteric coupling in proteins. *Proc. Natl Acad. Sci. USA*, **104**, 8311–8315.
54. Luo, W., Ng, W. W., Jin, L. H., Ye, Z., Han, J. & Lin, S. C. (2003). Axin utilizes distinct regions for competitive MEKK1 and MEKK4 binding and JNK activation. *J. Biol. Chem.* **278**, 37451–37458.
55. Liu, J., Xing, Y., Hinds, T. R., Zheng, J. & Xu, W. (2006). The third 20 amino acid repeat is the tightest binding site of APC for beta-catenin. *J. Mol. Biol.* **360**, 133–144.
56. Tompa, P., Fuxreiter, M., Oldfield, C. J., Simon, I., Dunker, A. K. & Uversky, V. N. (2009). Close encounters of the third kind: disordered domains and the interactions of proteins. *BioEssays*, **31**, 328–335.
57. Martin, J. & Dufour, J. F. (2008). Tumor suppressor and hepatocellular carcinoma. *World J. Gastroenterol.* **14**, 1720–1733.
58. Cabrita, L. D., Gilis, D., Robertson, A. L., Dehouck, Y., Rooman, M. & Bottomley, S. P. (2007). Enhancing the stability and solubility of TEV protease using *in silico* design. *Protein Sci.* **16**, 2360–2367.
59. Cheng, J., Randall, A. Z., Sweredoski, M. J. & Baldi, P. (2005). SCRATCH: a protein structure and structural feature prediction server. *Nucleic Acids Res.* **33**, W72–W76.
60. Linding, R., Jensen, L. J., Diella, F., Bork, P., Gibson, T. J. & Russell, R. B. (2003). Protein disorder prediction: implications for structural proteomics. *Structure*, **11**, 1453–1459.
61. Linding, R., Russell, R. B., Neduva, V. & Gibson, T. J. (2003). GlobPlot: exploring protein sequences for globularity and disorder. *Nucleic Acids Res.* **31**, 3701–3708.
62. Yang, Z. R., Thomson, R., McNeil, P. & Esnouf, R. M. (2005). RONN: the bio-basis function neural network technique applied to the detection of natively disordered regions in proteins. *Bioinformatics*, **21**, 3369–3376.
63. Dosztanyi, Z., Csizmok, V., Tompa, P. & Simon, I. (2005). IUPred: web server for the prediction of intrinsically unstructured regions of proteins based

on estimated energy content. *Bioinformatics*, **21**, 3433–3434.
64. Romero, P., Obradovic, Z., Li, X., Garner, E. C., Brown, C. J. & Dunker, A. K. (2001). Sequence complexity of disordered protein. *Proteins*, **42**, 38–48.
65. Pollastri, G. & McLysaght, A. (2005). Porter: a new, accurate server for protein secondary structure prediction. *Bioinformatics*, **21**, 1719–1720.
66. Combet, C., Blanchet, C., Geourjon, C. & Deleage, G. (2000). NPS@: network protein sequence analysis. *Trends Biochem. Sci.* **25**, 147–150.
67. Jones, D. T. (1999). Protein secondary structure prediction based on position-specific scoring matrices. *J. Mol. Biol.* **292**, 195–202.
68. Rost, B., Yachdav, G. & Liu, J. (2004). The PredictProtein server. *Nucleic Acids Res.* **32**, W321–W326.